

Aerosol-Derived Bimetallic Alloy Powders: Bridging the Gap[†]

Barr Halevi,[‡] Eric J. Peterson,[‡] Andrew DeLaRiva,[‡] Ese Jeroro,[§] Vanessa M. Lebarbier,^{||} Yong Wang,^{||} John M. Vohs,^{||} Boris Kiefer,[⊥] Edward Kunkes,[#] Michael Havecker,[#] Malte Behrens,[#] Robert Schlögl,[#] and Abhaya K. Datye^{*‡}

Department of Chemical & Nuclear Engineering and Center for Microengineered Materials, MSC01 1120, University of New Mexico, Albuquerque, New Mexico 87131-0001, Department of Chemical and Biomolecular Engineering, University of Pennsylvania, Philadelphia, Pennsylvania 19104, Institute for Interfacial Catalysis, Pacific Northwest National Laboratory, Richland, Washington 99352, Department of Physics, New Mexico State University, Las Cruces, New Mexico 88003, and Department of Inorganic Chemistry, Fritz-Haber-Institute of the Max-Planck-Society, Faradayweg 4-6, D-14195 Berlin, Germany

Received: May 1, 2010; Revised Manuscript Received: August 15, 2010

We present aerosol-derived alloy powders as a uniquely useful platform for studying the contribution of the metal phase to multifunctional supported catalysts. Multimetallic heterogeneous catalysts made by traditional methods are usually nonhomogenous while UHV-based methods, such as mass selected clusters or metal vapor deposited on single crystals, lead to considerably more homogeneous, well-defined samples. However, these well-defined samples have low surface areas and do not lend themselves to catalytic activity tests in flow reactors under industrially relevant conditions. Bimetallic alloy powders derived by aerosol synthesis are homogeneous and single phase and can have surface areas ranging 1–10 m²/g, making them suitable for use in conventional flow reactors. The utility of aerosol-derived alloy powders as model catalysts is illustrated through the synthesis of single phase PdZn which was used to derive the specific reactivity of the L1₀ tetragonal alloy phase for methanol steam reforming. Turnover frequencies on unsupported PdZn were determined from the experimentally determined metal surface area to be 0.21 molecules of methanol reacted per surface Pd at 250 °C and 0.06 molecules of CO oxidized to CO₂ per surface Pd at 185 °C. The experimentally measured activation energies for MSR and CO-oxidation on PdZn are 48 and 87 kJ/mol, respectively.

Introduction

Industrial heterogeneous catalysts are typically multifunctional¹ and involve synergistic contributions from several metallic^{2–5} components as well as the catalyst support. Unraveling the contributions of each of these components has traditionally relied on two approaches: study of metallic particles on different powder supports or the surface science approach of synthesizing the metallic phase in the form of a single crystal or a thin film. The first approach requires the synthesis of metallic particles of interest on different high surface area powder supports and through comparison of the supported catalyst reactivity it is possible to deconvolute the contribution of the supported metallic particles from the supports. The synthesized catalysts can be tested at industrially relevant pressures and temperatures, and in situ characterization techniques such as IR and XAS spectroscopies can be employed. This approach suffers from the limited compositional, size, and phase homogeneity in the supported catalysts. However, sample inhomogeneity can sometimes mask the effects of the support and thus hinder identification of the catalytically active species. It is possible to improve the compositional uniformity by depositing well-defined nanoparticles via UHV techniques on

single crystal oxide surfaces, but catalytic testing of these model catalysts is limited to batch reactor studies.⁶

The second approach to understanding multifunctional catalysts is the surface science approach where well-defined metal single-crystal substrates with surface areas of 1–10 cm² are used as model catalysts. This approach allows for well-characterized systems that can be tested in single-turnover experiments. This approach does not traditionally allow the multiple-turnover or high-pressure experiments that are needed to investigate industrially relevant reaction conditions. While a high pressure batch reactor can be coupled to a surface science reaction system, it is still difficult to study phenomena such as catalyst deactivation or to test catalysts under high pressures and with industrially relevant feeds that may contain trace level impurities.^{7,8} Multimetallic thin film catalysts have recently been used as model catalysts, but it has been found that catalytic activity changes with the thickness of bimetallic layers,^{9,10} and these thin films can undergo structural changes under reaction conditions. It is therefore necessary to find an approach that bridges the gap between model catalysts studied used in surface science experiments and those that can be tested in a conventional flow reactor under industrially relevant conditions.

We present a novel form of a model catalyst synthesized via aerosol synthesis that makes it possible to bridge the materials/pressure gap between UHV surface science and conventional heterogeneous catalyst studies. Aerosol synthesis allows us to prepare homogeneous, well characterized, unsupported metallic powders that have surface areas of 1–10 m² per gram. These surface areas are sufficiently high to allow reactivity testing in flow reactors under industrially relevant pressures and flow rates.

[†] Part of the “D. Wayne Goodman Festschrift”.

^{*} To whom correspondence should be addressed. E-mail: datye@unm.edu.

[‡] University of New Mexico.

[§] University of Pennsylvania.

^{||} Pacific Northwest National Laboratory.

[⊥] New Mexico State University.

[#] Fritz-Haber-Institute of the Max-Planck-Society.

For example, a 20 mg sample of the PdZn powder used in this work provides us with over 1000 cm² of active metal surface area, which is more than enough for use at the space velocities normally used for testing heterogeneous catalyst. Since the BET surface area of the powder is known, we can now determine the specific reactivity of the bimetallic phase, free of the support. Hence, the contributions of the metal and support components can be elucidated. Thus aerosol-derived bimetallic powders provide an innovative approach to measuring and understanding the contribution of the metallic component in complex, multi-component technical catalysts under industrially relevant conditions.

The system we have studied is Pd/ZnO, which has been shown to be a highly effective catalyst for methanol steam reforming exhibiting good rates and 95%+ selectivities to CO₂ while not suffering from some of the drawbacks of the commercially prevalent Cu/ZnO/Al₂O₃ system.^{11–13} The Pd/ZnO system has been extensively studied but the nature of the catalytically active phase is still being debated. It was found that a PdZn phase forms *in situ* under steam reforming conditions and was therefore suggested that the PdZn phase is responsible for much of the observed activity of Pd/ZnO.¹¹ The PdZn phase can also be formed by first reducing Pd/ZnO *ex situ*, and it was found that content of PdZn in the reduced Pd/ZnO did not correlate with the overall methanol steam reforming activity.^{11,14,15} Subsequent studies have shown that more faceted ZnO powder supports improve reactivity¹⁶ and that selectivity to CO₂ decreases dramatically for PdZn particles smaller than ~5 nm,¹⁵ likely due to increased reverse-water-gas shift activity.¹⁷ The Pd/ZnO system is therefore a complex system where support, bimetallic phase and particle size have all been shown to contribute to catalytic performance. It was indeed surprising that overall conversion of the Pd/ZnO catalysts was unaffected by heating to higher temperatures beyond 573 K where the surface area of the PdZn phase was decreasing due to increased crystallite size.^{15,18} It is therefore necessary to understand the inherent reactivity of the PdZn phase so that comparisons with supported catalysts can help elucidate the role of the ZnO support. We have recently shown that PdZn powders made from aerosols of Pd and Zn salt solutions followed by decomposition and H₂ reduction yield phase pure PdZn (via X-ray and neutron diffraction).¹⁹ The catalytic activity of these unsupported PdZn powders is examined in this work so as to establish the specific reactivity of the PdZn phase in the steam reforming of methanol. For comparison, we have also measured CO oxidation rates on these powders so that these measurements could be used in future work to provide an independent measure of the catalytically active surface area in supported catalysts.

Experimental Section

PdZn aerosol-derived catalysts were made using palladium and zinc nitrate (Aldrich, 99.99%+) dissolved in 10% nitric acid. The nitrate salt mixture was atomized to produce droplets that dried as they passed through a furnace, and the droplets were collected on a filter. The collected powder was reduced at 500 °C in flowing 5% H₂ for 4 h. The reduction temperature was selected to ensure rapid formation of the PdZn L1₀ phase without any significant loss of Zn due to evaporation.¹⁹ For comparison, PdZn precipitated catalysts were prepared using palladium and zinc nitrate (Aldrich, 99.99%+) dissolved in 10% nitric acid and allowing the mixture to evaporate to dryness. The nitrate salt mixture was dried at 120 °C in air, oxidized at 350 °C in air for 3 h, and reduced at 500 °C in flowing 5% H₂ for 2 h. PdO powder (Sigma, 99.99 wt %) was calcined in air

at 350 °C for 3 h. All catalysts were pelletized and sieved to 106–260 µm, and then 20 mg of the sieved powder was loaded in a 1.7 mm ID reactor tube with a packed catalyst bed length of ~20 mm and ~10 mg quartz wool plug on either end of the catalyst bed.

Reactivity studies were performed in a reactor tube placed in a Varian 3400 GC oven that served as a temperature programmable furnace for the reactor, a reactor feed system, and a Varian 3800 GC equipped with TCD detector for the analysis of the products. The reactor feed system used MKS mass flow controllers and a high pressure pump-fed vaporizer system for introducing liquid reactants such as water and methanol. Samples were treated *in situ*, and then tested for MSR activity at 250 °C until steady state performance was achieved. Oxidation, reduction, and oxidation and reduction treatments followed by MSR at 250 °C were used to evaluate the catalyst deactivation and regeneration. Once steady MSR performance was reached, the MSR reactivity was measured over a range of temperatures, followed by CO-oxidation measurements to quantify the surface Palladium sites. The sequence of experiments, i.e., 3 h of MSR at 250 °C, followed by catalyst pretreatment, followed by CO-oxidation measurements, and then finally followed by MSR at 250 °C, was repeated to provide a test for catalyst stability. Methanol steam reforming activity was evaluated using a syringe that feeds a 0.2 mL/h premixed water/methanol mixture (molar ratio of 1.1:1) aerated with 77.5 sccm preheated helium through a vaporizer operating at 200 °C and introduced directly into the reactor. Prior to activity tests, the catalyst was oxidized *in situ* for 60 min using 50 sccm 2%O₂/He at 250 °C and then reduced *in situ* under 50 sccm 5%H₂/He for 120 min at 250 °C.¹⁹ The product gases were analyzed using a series/bypass configured mol-sieve/capillary column in a Varian CP-3800 GC equipped with TCD detector. CO oxidation was carried out in the same system using flows of 30 sccm 5%CO/He, 50 sccm 2%O₂/He.

CO oxidation reactivity studies were duplicated in a different reactor system which made use of a micro GC allowing us to study the light-off curves for CO oxidation. This second reactor system also used MKS flow controllers to feed 30 sccm 5%CO/He, 50 sccm 2%O₂/He to a temperature programmable furnace monitored by a Varian CP-4800 Micro-GC. Prior to activity tests, the catalyst was oxidized *in situ* for 60 min using 50 sccm 2%O₂/He at 250 °C then reduced *in situ* under 50 sccm 5%H₂/He for 120 min at 250 °C.

High vacuum TPD experiments were conducted in a diffusion-pumped system equipped with VGQ quadrupole mass-spectrometer, temperature controlled radiatively heated sample basket, cold-cathode gage for pressure measurement, and leak valve for introduction of probe gases. Approximately 20 mg of the powder sample was loaded in the basket, pumped down for 4 h, then heated to 350 °C in 2 Torr H₂ to remove adsorbed environmental gases, reduce the sample, and form a PdZn alloy. Alloy formation using this pretreatment was confirmed by XRD. Samples were exposed to 2 Torr gas for 30 min and then pumped down for 4 h. Samples were then heated at 10 K/min up to 427 °C and desorption products monitored by quadrupole mass-spectrometer.

Nitrogen adsorption was measured at 77 K with in a Micromeritics Gemini System and Quantachrome Autosorb 1-C/TCD. The samples were treated at 120+ °C for 3+ h under vacuum before measurements. The surface areas were determined from adsorption values for five relative pressures (P/P_0) ranging from 0.05 to 0.2 using the BET method. Chemisorption was carried out in the Autosorb 1-C/TCD at 250 °C using a

pretreatment regimen of in situ oxidation for 60 min, followed by reduction in H₂ for 120 min, followed by 30 min of evacuation at 250 °C. Analysis was based on total H₂ uptake over 20–300 Torr extrapolated to zero pressure.

Thermogravimetric analysis was carried out in a TA Instruments Q600-SDT flowing gas thermogravimetric analyzer equipped with Pfeiffer Thermostar Quadruple Mass Spectrometer. Experiments were carried out under 50 sccm of compressed air, 7%H₂/N₂, or N₂.

Scanning and high-resolution transmission electron microscopy (STEM and HRTEM) were performed on a JEOL 2010F FASTERM field emission gun scanning transmission electron microscope equipped with EDS. The probe size for analytical work was 1.0 nm and accelerating voltage was 200 kV. Scanning electron microscopy (SEM) was performed on a Hitachi S-5200, with a resolution of 0.5 nm at 30 kV and 1.7 nm at 1 kV, and EDS was carried out at 20 kV using a PGT Spirit system.

X-ray powder diffraction spectra were recorded using Scintag Pad V diffractometer with DataScan 4 software (from MDI, Inc.) for system automation and data collection. Cu K α radiation (40 kV, 35 mA) was used with a Bicron Scintillation detector (with a pyrolytic graphite curved crystal monochromator). Data sets were analyzed with Jade 9.5 Software (from MDI, Inc.) using the ICDD (International Center for Diffraction Data) PDF2 database (rev. 2004) for phase identification.

X-ray photoelectron spectroscopy was performed on a Kratos Axis Ultra X-ray photoelectron spectrometer. Spectra were recorded under the operating pressure of around 2×10^{-9} Torr using a monochromatic Al K α source operating at 300 W with charge compensation. Broad-range spectra were acquired at 80 eV pass energy, whereas high resolution spectra were acquired at a pass energy of 20 eV. Ambient pressure XPS experiments were carried out at ISISS, the catalysis beamline of the FHI at the third generation synchrotron BESSY II (Helmholtz-Zentrum Berlin). The powder samples were pressed into self-supporting discs >0.5 mm thick that were mounted in the in situ heated holder and exposed to gases at up to 1 Torr. Spectra were generated using incident photon energies of 120 eV above monitored B.E. energy window and adjusted for beamline photon flux variations. Incident photon energies were 120 eV for Zn3d/VB, 410 eV for C1s, 460 eV for Pd3d, 650 eV for O1s, and 1250 eV for Survey scans. Pass energy was 20 eV for survey and 10 eV for detailed scans, respectively, and the exit slit of the beamline was 111 μ m. The sample was mounted and chamber evacuated and survey and detailed scans were first acquired. The sample was then heated to 250 °C in the presence of flowing 0.25 mbar (or 0.19 Torr) hydrogen. Quantification was performed using CasaXPS software. Subtraction of a Shirley background was followed by charge referencing of all spectra to gold powder dabbed near the sample for ex-situ XPS, carbon at 285 eV, and the Fermi-level. Sensitivity factors were provided by the manufacturer or referenced to published data. Curve-fitting was carried out using individual peaks with 70% Gaussian/30% Lorentzian line shape and widths and binding energies were constrained to best experimental fittings of reference Pd and PdO materials.

We augmented our experiments with calculations that are based on density-functional-theory²⁰ as implemented in the software package VASP.^{21–24} Electronic exchange and correlations were treated at the GGA level within the parametrization of Perdew, Burke, and Ernzerhof.²⁵ The interactions between electrons and nuclei were described within the PAW formalism.^{26,27} The electronic configurations (core radii in atomic units are given in parentheses) were 5s²4p⁶3d⁸ (2.300 a_B), 3d¹⁰4s² (2.300

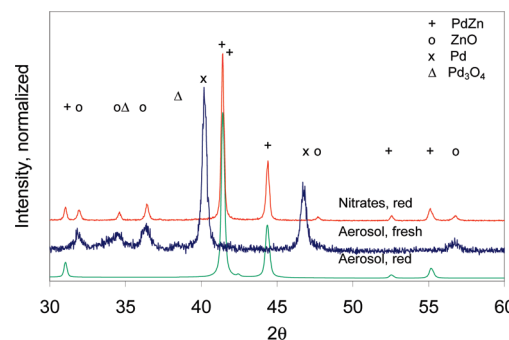


Figure 1. X-ray powder diffractogram of samples made from the aerosol route as prepared and after hydrogen reduction. The precipitated nitrate solution, after reduction shows the presence of ZnO which was not seen in the aerosol derived reduced powder.

aB), 2s²2p² (1.500 a_B), and 2s²2p⁴ (1.520 a_B), for Pd, Zn, C, and O, respectively. The Pd and PdZn(111) surfaces were modeled as four layer slabs each layer containing 16 atoms, Figure 10, using a Γ -centered $2 \times 2 \times 1$ k-point grid. The PdZn(111) surfaces were derived from the tP4 representation of stoichiometric and fully ordered tetragonal Pd₅₀Zn₅₀ alloy.²⁸ All calculations were performed using a planewave energy cutoff of 400 eV. The atoms in the bottom two layers were held fixed at the DFT optimized bulk equilibrium positions, the atoms in the top two layers were allowed to relax, similar to previous work on PdZn.²⁹ The calculated equilibrium lattice parameter for fcc-Pd is $a = 3.952$ Å (14 × 14 × 14 k-point grid), and for tetragonal, stoichiometric, and ordered PdZn, we obtain $a = 4.127$ Å and $c = 3.417$ Å (14 × 14 × 16 k-point grid). For comparison the experimental lattice parameters are, $a = 3.891$ Å and $a = 4.100$ Å and $c = 3.295$ Å, for Pd and PdZn, respectively.^{28,30} This slight overestimation of the lattice parameters is typical for GGA calculations.²⁷ Slabs were separated by a 14 Å vacuum layer in order to reduce slab–image slab interactions, similar to previous work on transition metal (111) surfaces,³¹ and spurious long-ranged dipole interactions were corrected for by introducing a compensating dipole layer.^{32,33} The Fermi level was broadened using first order Methfessel and Paxton smearing ($\sigma = 0.1$ eV).³⁴ CO in the gas phase was optimized in an orthogonal anisotropic box of dimensions 10 Å × 11 Å × 12 Å using a single k-point (Γ -point). The relaxed C–O bond distance is 1.143 Å.. Following Blyholder's model,³⁵ the initial configuration of CO was such that carbon was facing the surface. We compensated for the known overbinding of DFT by following the method outlined in refs 21 and 25. The required C–O stretching frequencies were calculated from a reduced dynamical matrix that included only the vibrations of the CO molecule. The resulting (6 × 6) dynamical matrix was determined by finite differences from displacements by ± 0.01 Å of carbon and oxygen. Binding energies were evaluated from the internal energies as $E_B = E(\text{surface-CO}) - E(\text{surface}) + E(\text{CO})$. Zero-point motion and thermal effects were neglected since their magnitude is small compared to the calculated binding energies and almost independent of the binding site.³¹ For CO adsorption we used top, bridge, fcc, and hcp hollow sites on Pd(111) and seven sites on PdZn(111) as shown in Figure 10.

Results and Discussion

The X-ray diffraction pattern of the powders is presented in Figure 1 and shows that the aerosol-derived powder is initially composed of Pd, ZnO, and small amounts of Pd₃O₄. Reduction in flowing hydrogen at 500 °C for 4 h leads to the formation of

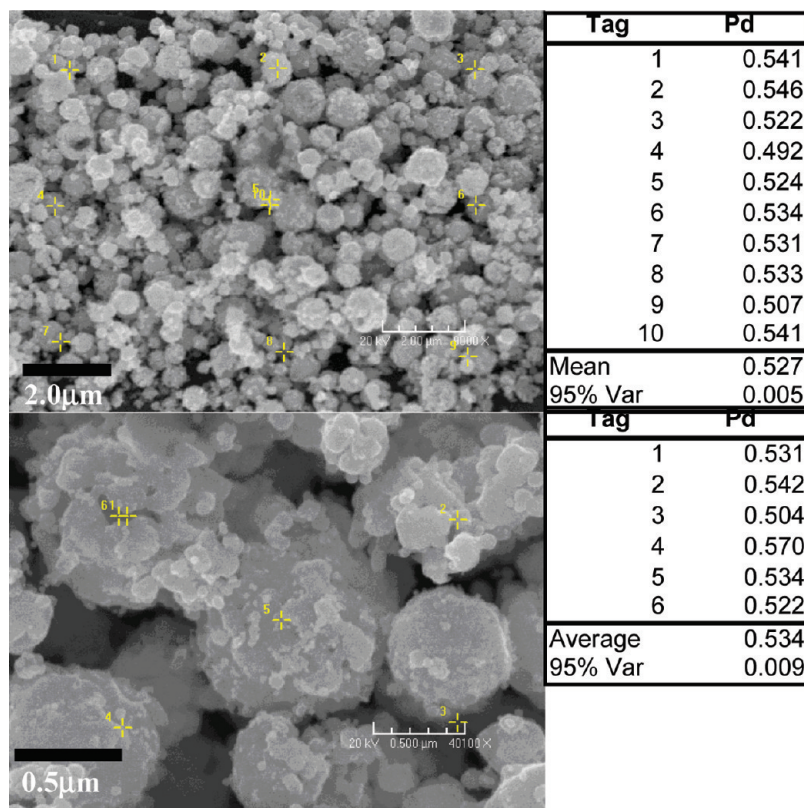


Figure 2. SEM/EDS spot analysis micrograph of aerosol-derived phase pure PdZn alloy.

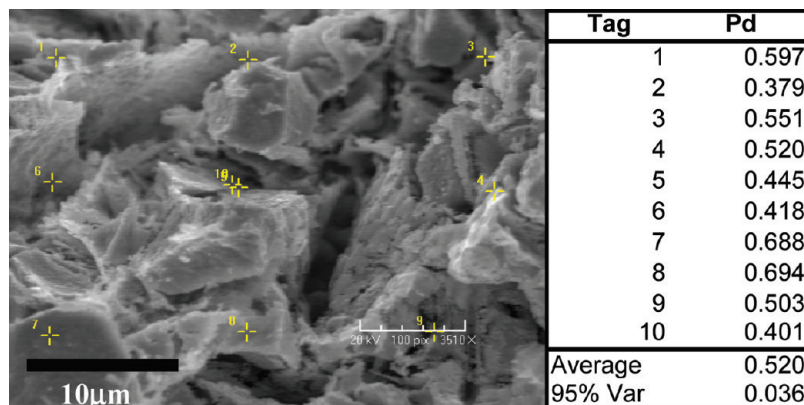


Figure 3. SEM/EDS micrograph of PdZn made by drying Pd + Zn nitrate solution.

phase pure PdZn. In contrast, the material made from reduction of the dried nitrate precursors is composed of PdZn and as much as 10% ZnO indicating incomplete alloy formation.

This suggests that generation of an aerosol creates small droplets that are well mixed and are more easily reduced and alloyed whereas more traditional coimpregnation could lead to compositional nonuniformities. Scherrer analysis suggests crystallite sizes of 44 and 48 nm for aerosol-derived and nitrate decomposition-derived powders. The diffraction-estimated crystallite size for the aerosol-derived PdZn suggests a surface area of $15 \text{ m}^2/\text{g}$ based on an assumption of spherical particles.³⁶ The measured BET surface area is much lower $5.85 \text{ m}^2/\text{g}$, which would arise from particles with 250 nm average particle size. It is therefore clear that each particle is composed of multiple crystallites and hence the XRD-average crystallite size cannot be used for estimating the available surface area of the unsupported PdZn.

SEM/EDS. SEM/EDS micrographs and analysis summary displayed in Figure 2 demonstrate that the aerosol-synthesis

process produces regular spherical aggregates with diameters on the order of 200 nm composed of 20–60 nm irregularly shaped particles and grains and some less well intercalated particles of the same size. The observed SEM/EDS composition of the aerosol-derived powders is 52.7 with a variance of 0.5 atom % Pd, consistent with the 51.6 atom % Pd mean composition as determined by XRF. The compositional variability is consistent with the inherent limitations of the SEM/EDS technique and the standard deviation of less than 1% of the mean composition as determined by microprobe analysis of similarly produced powders.¹⁹ In contrast, the material made by decomposing a nitrate solution directly, seen in Figure 3, is much less homogeneous with a mean composition of 52.0 with a variance of 4.0 atom % Pd.

STEM/EDS. STEM/EDS micrographs and compositional line scan analysis with a 1 nm probe, Figure 4, confirm that a 1:1 Pd:Zn ratio is maintained throughout the PdZn particles on a 1–2 nm scale and indicate PdZn crystallite sizes range from 10–60 nm, in agreement with the 44 nm crystallite size inferred

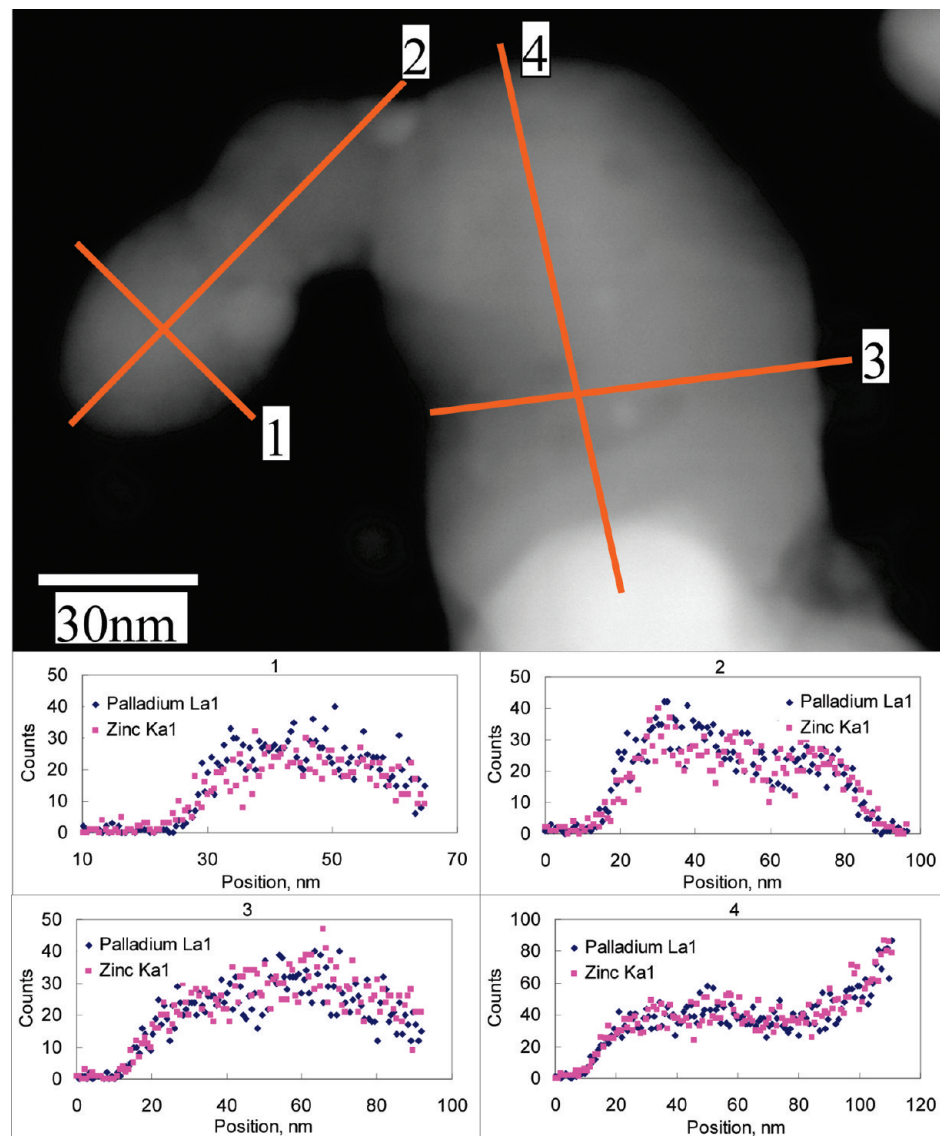


Figure 4. Z-contrast image with indicated EDS linescan positions and the EDS calibrated atomic compositional linescan profiles for Pd La α 1 and Zn Ka α 1 lines.

from XRD. STEM images combined with XRD, BET, and SEM indicate that the aerosol-derived PdZn powder is composed of irregularly shaped 10–60 nm crystallites that sinter to form very slightly porous spherically shaped particles with diameters of 0.5–2.0 μ m.

HRTEM. HRTEM micrographs were acquired to confirm that the PdZn nanoscale structure matches the bulk structure established by XRD and NPD. HRTEM was also used to study the surface structure of the PdZn powders. A representative low magnification image of several PdZn particles in Figure 5A shows rounded, 20–60 nm dense particles with fairly even shading indicating homogeneous density within the particles and confirming that the primary particles are non porous as seen by STEM. Also evident are lighter-shaded shells coating all of the particles. Higher magnification imaging, exemplified in Figure 5B, shows that the PdZn particles are uniformly covered by ~2–3 nm of a crystalline phase. These crystalline surface films show small single crystal domains that can be indexed to ZnO. Also evident are the denser core PdZn particles that most often display the prominent PdZn (−1,0,1) family of planes. The PdZn sample is therefore seen to be composed of sintered agglomerates made up of 20–60 nm single crystal particles of the PdZn L1₀ phase as inferred from the XRD powder patterns. The ZnO

thin film coating the particles is likely formed over time due to preferential oxidation of Zn by air. To confirm that the ZnO thin film is eliminated by reduction, the PdZn sample was reduced for 2 h at 250 °C in flowing 5% hydrogen, the same reduction used for catalyst activation during reactivity testing, then passivated in flowing nitrogen with ~50 ppm oxygen for 1 h and examined by HRTEM after approximately 1 h of air exposure. Low magnification images of several particles in the reduced sample, Figure 5C, show that the reduction treatment has essentially eliminated the ZnO surface film leaving PdZn exposed on the surface. High magnification images, Figure 5D, confirm that most of the ZnO film has been lost, but some patches of ZnO are still seen on the PdZn cores. HRTEM therefore suggests that the surface structure of the PdZn sample in its reduced state likely matches the bulk structure, and that the ZnO that forms on the surface after exposure to air are easily reduced under the conditions used for in situ catalyst reactivity measurements.

Ambient Pressure XPS. Ambient pressure XPS spectra are displayed in Figure 6. The aerosol-derived sample was mounted, the chamber was evacuated, and survey and detailed scans were acquired. The sample was then heated to 250 °C in the presence of flowing 0.25 mbar (or 0.19 Torr) hydrogen. The survey scan

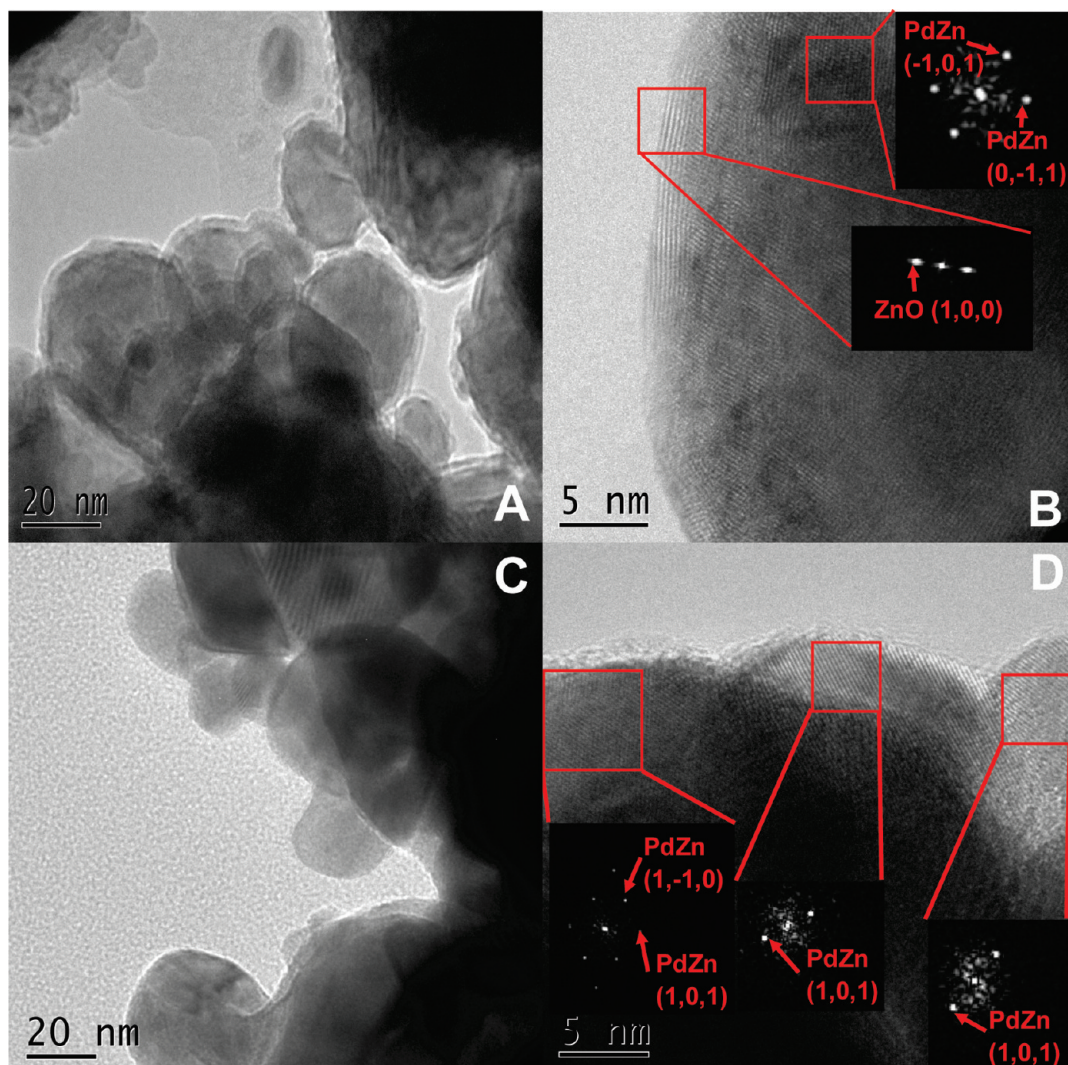


Figure 5. HRTEM of PdZn samples. (A) Lower magnification image of a powder exposed to air for several months showing a lower contrast surface layer covering all of the metal particles and (B) high magnification image showing the lower contrast surface film is a 2–3 nm thick film indexed to ZnO (1,0,0) that covers a dense particle indexed to PdZn. The ZnO surface layer is reduced and only sparse patches of ZnO remain after reduction using the same conditions used for *in situ* catalyst pretreatment (2 h at 250 °C in flowing 5% Hydrogen) followed by air exposure as seen in (C) the lower magnification image showing the absence of any surface oxide films and (D) the high magnification image of the reduced sample.

revealed palladium, zinc, oxygen, and carbon were present on the sample surface. The Pd3d peak assignments were based on Pd to surface PdO shift of 1.6 eV at oxygen mbar pressure range^{37,38} and best-fit 0.7 eV shift for the bimetallic Pd peak. The Pd3d3/2 peaks were fitted using a 5.3 eV spin-orbit splitting between 5/2 and 3/2 peaks. Pd3d spectra show the peak shifts from metallic Pd to PdZn alloy upon reduction at 250 °C. Zn3d spectra similarly show the presence of alloy upon reduction with a shift of the peak from Zn oxide at 10.2^{39–41} to PdZn alloy at 9.3 eV along with coexistence of ZnO on the surface. O1s spectra collected from 120 eV photoelectrons indicate that oxygen content dropped by half after reduction while the peak shape was unchanged. The change in area but not shape is consistent with adventitious adsorbates being eliminated but also suggests that oxygen is incorporated in the sample. The C1s peak area is minute, consistent with adventitious adsorbates only and some minor systematic contamination. Surface sensitive analysis using the high resolution Pd3d, Zn3d, C1s, and O1s scans with incident energies set so that the photoelectron kinetic energy is 120 eV for all transitions shows Pd/Zn ratio of 0.16 and O/Zn ratio of 0.28. Thus it is possible

to determine that the surface of the sample is composed of 70% Zn, 20%O, and 10%Pd. Since the mean free path for 120 eV photoelectrons used in the high resolution scans is approximately 0.3 nm,⁴² the depth probed by the high resolution scans is ~1.0 nm. As SEM/EDS analysis shows a 50:50 ratio of Pd:Zn and Zn is more oxophilic than palladium, it is likely that the outer surface of the powder is ZnO. If 1:1 Pd:Zn ratio is assumed for the Pd then 20% of the probed depth must be composed of PdZn with the rest being 60% Zn and 20% is O. This indicates that treatment of the PdZn sample in 0.19 Torr at 250 °C for 30 min results in a surface that is likely covered in 2–3 ML of substoichiometric ZnO. The ambient pressure XPS reduction confirms that the surface of these powders also shows alloyed PdZn along with surface ZnO, which was caused during air exposure of the samples and was observed by HRTEM as well. We conclude that the short reduction treatment (30 min) at low pressure during the ambient XPS experiment leads to only partial reduction of the PdZn powder samples. However, even this partial reduction is sufficient for alloying the surface metallic Pd with Zn even while ZnO film elimination is incomplete. The ease of Pd alloying confirms that Pd alloys readily with Zn.

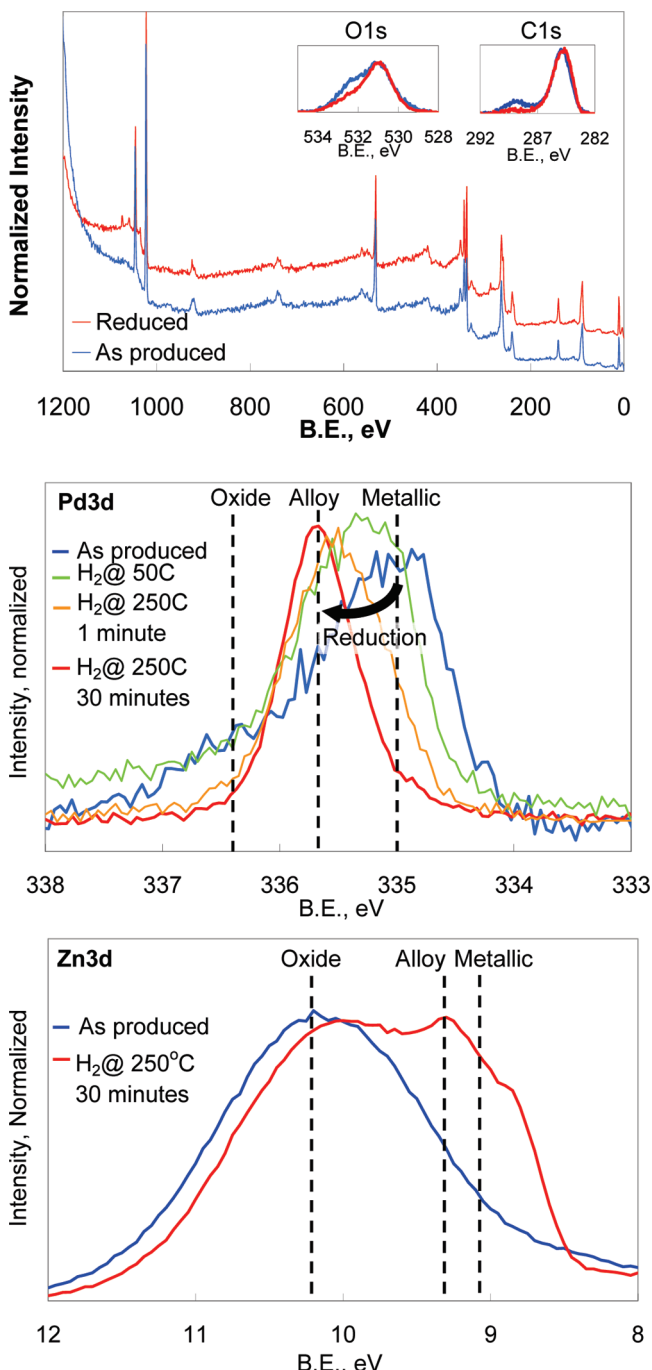


Figure 6. Ambient pressure XPS survey with inset C1 and O1s, as well as Pd3d and Zn3d spectra of PdZn air-exposed and after reduction in 0.25 mbar (or 0.19 Torr) flowing hydrogen at 250 °C.

The reduction treatment during catalytic reaction measurements is more severe (2 h at 250 °C with 23 Torr H₂) and it is therefore likely that surface ZnO films are completely removed, but confirmation will come only from future work at the BESSY beamline.

Temperature Programmed Desorption. Temperature programmed desorption of CO and methanol in vacuum, Figure 7, shows that CO dosed on unsupported PdZn adsorbs at room temperature and then desorbs at 150 °C. Applying Redhead analysis suggests E_{des} for CO from PdZn is therefore 120 kJ/mol. Thus, it is clear that addition of Zn to Pd serves to weaken CO binding to Pd. In UHV CO TPD experiments conducted on PdZn alloys formed from Zn/Pd(111) and cooled to 100 K,⁴³ it was observed that increasing amounts of Zn deposited on

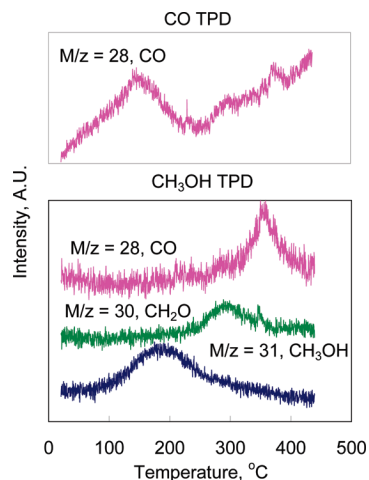


Figure 7. Vacuum TPD of CO and temperature programmed decomposition of CH₃OH on PdZn alloy powder.

Pd(111) reduced both the amount of CO adsorbed and temperature of desorption for CO. In the single crystal work it was found that CO desorption occurred well below room temperature when more than 0.25 ML Zn was deposited. It is possible that the differences observed between CO desorption from Zn/Pd(111) and PdZn are due to the vastly increased dosing pressure used on the powder samples. But it has also been shown recently that monolayer alloys can differ in their catalytic behavior from multilayer alloys^{9,10} and from the results reported here, it appears that bulk metal powders may be even different from multilayer alloy films. The sites created by deposition of Zn on Pd(111) may not be the same as the sites present on bulk PdZn alloys.

TPD experiments were also used to monitor the decomposition of methanol on the bulk PdZn sample. Methanol adsorbs readily at room temperature leading to desorption products of CH₃OH at 190 °C, CH₂O at 300 °C, and CO at 350 °C. The three desorption products are consistent with a reaction pathway where methanol adsorbs dissociatively to form adsorbed methoxide and hydride. The methoxide can recombine with hydride and desorb as methanol, undergo dehydrogenation to formaldehyde, or further decompose to CO. First order Redhead desorption analysis yields desorption energies of 130, 165, and 180 kJ/mol for the three desorption products. These relatively high desorption energies suggest that all three desorption products are reaction limited⁴⁴ and therefore can be assigned activation energies corresponding to the desorption energies. The reaction pathway for methanol decomposition on PdZn is therefore consistent with that previously suggested by Neyman et al.^{44,45} where in the absence of water—methanol adsorbs to make methoxide, dehydrogenates to make formaldehyde or formate, and further dehydrogenates to CO. Thus it is possible to conclude that the desired sequential dehydrogenation steps in the decomposition of methanol on bulk PdZn have the activation energies 165 kJ/mol for making formaldehyde and 180 kJ/mol for making CO. UHV methanol decomposition experiments using PdZn thin films formed from Zn sputtered/Pd(111) and cooled to 100 K⁴⁴ observed methanol production at 200 °C for near stoichiometric PdZn compositions, similar to the methanol production observed on bulk PdZn in this study. However, formaldehyde production was not observed for Zn converges beyond 0.1 ML and CO desorbed at approximately room temperature for near stoichiometric PdZn films. Our results suggest that the catalytic behavior of thin film single crystal model catalysts may differ from that observed on bulk PdZn materials.

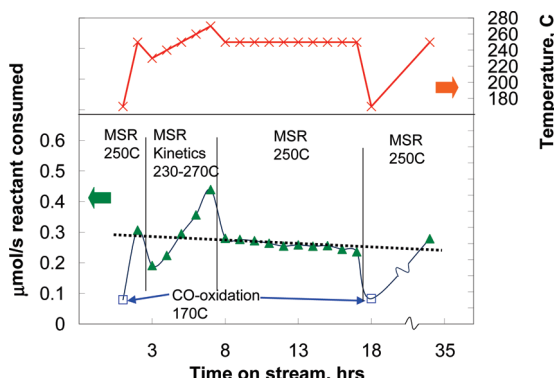


Figure 8. On-stream catalytic performance of PdZn under MSR (Δ) and CO oxidation (\square). Dashed line illustrates MSR performance at 250 °C over time. The reactor temperature was changed over the course of this extended run to alternately perform CO oxidation and MSR reactivity measurements on the same catalyst. As shown here, there is no induction time after switching to MSR reactivity, whereas CO oxidation is able to reverse the modest deactivation observed at 250 °C during MSR.

Catalytic Reactivity. After in situ pretreatment, the bulk PdZn was tested for MSR and CO oxidation. The catalytic performance illustrated in Figure 8 shows a typical catalyst test that lasted over several days wherein the MSR reaction runs were alternated with in situ CO-oxidation. The long-term tests show that there is slight deactivation of PdZn under MSR reaction conditions at 250 °C. MSR selectivity to CO_2 remained high at 98%+ up to 270 °C. Since MSR reaction rate measurements were alternated with CO oxidation tests where we may cause oxidation of the catalyst, it is interesting to note there is no induction time after switching the reaction mixture back to MSR. The MSR product sampling occurred within 1 min of switching the reactor feed from CO oxidation to MSR feeds. The results show that the CO oxidation measurements at temperatures up to 200 °C, where we observed 100% conversion of CO, had no detrimental impact on MSR reactivity but rather helped to regenerate the catalyst. The reactivity of these bulk PdZn powders demonstrate the remarkable stability of this intermetallic alloy phase to surface oxidation that might have been expected to occur during CO oxidation.

As controls, we also tested the catalytic performance of ZnO, Pd, and PdO powders. Pd and PdO were found to be 100% selective to CO and ZnO was inactive under the MSR conditions used in this study. The observed activation energies for MSR and CO oxidation on PdZn are 48 and 87 kJ/mol, respectively. Since some comparisons of PdZn to Cu have been made in the literature, it is worthwhile to note that MSR activation energy on Cu is reported to be more than twice that found for PdZn,^{46–48} indicating that PdZn reaction kinetics are not comparable to Cu and therefore suggesting a different reaction mechanism for MSR on PdZn than on Cu. The observed activation energy of 87 kJ/mol for CO oxidation on PdZn is lower than the 103 kJ/mol activation energy reported for Pd/SiO₂,⁴⁹ which may be consistent with the lower binding energy for CO on PdZn. The results suggest that alloying zinc with palladium does not drastically alter the basic CO oxidation behavior of palladium and hence CO oxidation rate may serve as an in situ measure of the number of surface sites in PdZn catalysts. A more detailed study of CO oxidation kinetics on Zn modified Pd surfaces is underway.

To convert the observed reactivity of the catalyst to an explicit turnover frequency for MSR and CO oxidation on PdZn it is first necessary to measure the number of active sites in the

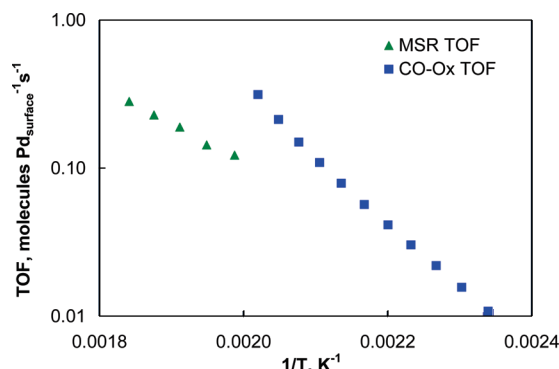


Figure 9. Turnover frequency (TOF) for reactant molecules consumed under MSR (Δ) and CO oxidation (\square) per surface palladium atom. The activation energies for the two reactions are 48 kJ/mol for MSR and 87 kJ/mol for CO oxidation.

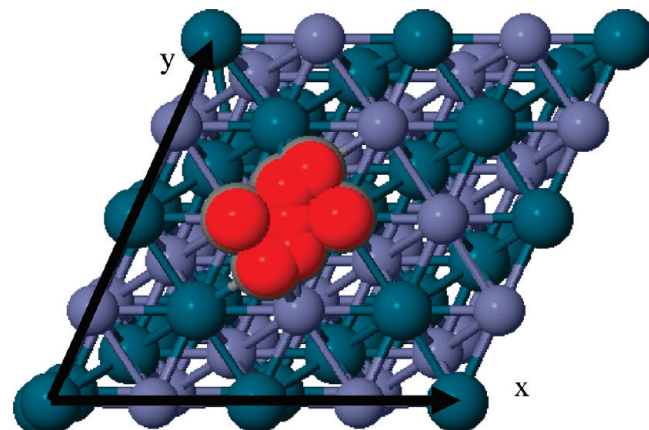


Figure 10. Top view of the initial positions for CO adsorption calculations on stoichiometric and ordered PdZn (1,1,1), x axis: [1,0,−1]; y axis [0,1,−1].

sample. The measurement of active sites is difficult for supported PdZn catalysts since stoichiometry of CO on Pd is variable and H₂ is known to absorb in Pd metal forming the beta Pd hydride. Hence estimates are generally derived from X-ray diffraction or electron microscopy or from H₂ chemisorption at elevated temperature. For the unsupported model catalysts described in this work it is possible to directly measure the surface area of the catalyst using physisorption measurements where no assumption has to be made about adsorption stoichiometry.

The PdZn sample in this work has a BET surface area of 5.85 m²/gr. Since palladium atoms are the likely active sites in PdZn, it is necessary to find the portion of the catalyst surface area that is palladium atoms so as to quantify per site reactivity. From the structure of PdZn and an assumed palladium atom area of 7.94 Å,²³⁶ we can estimate an active site density of 10.5 $\mu\text{mol Pd}_{\text{surface}}/\text{m}^2_{\text{PdZn}}$ or 62 $\mu\text{mol Pd}_{\text{surface}}/\text{g}_{\text{catalyst}}$ for the sample in this study. Confirmatory hydrogen chemisorption studies were carried out at 100 °C and 10–90 Torr so as to avoid beta hydride formation. The measured hydrogen uptake of 1.39 cc/g or 63 $\mu\text{mol/g}$, translates to 1.01 H/Pd based on the calculated palladium content of the surface, thus confirming the site density derived from BET surface area. The measured 62 $\mu\text{mol Pd}_{\text{surface}}/\text{g}_{\text{catalyst}}$ site density of the sample was then used to calculate the turnover frequencies displayed in Figure 9. The measured CO oxidation TOF on PdZn of 0.05 s⁻¹ at 180 °C is comparable to the 0.033 s⁻¹ TOF reported for monometallic palladium.⁴⁹ The recorded MSR TOF 0.12 s⁻¹ at 230 °C for PdZn is lower than the value of 0.8 s⁻¹ reported previously for supported samples by Ranganathan et al.,⁴⁵ but this previous study used a 7-fold

higher reactant concentration. The measured TOFs represent the first direct measurement of the catalytic performance of the PdZn phase. The relative MSR and CO oxidation activities of bulk PdZn will help provide a benchmark for further study of the role of ZnO on PdZn in supported catalysts.

Computational Work. Computational work has been used synergistically with single crystal model catalysts but it is difficult to extend the utility of ab initio method to powder catalysts because of the inhomogeneity of multimetallic supported catalysts. The ability to make phase-pure and unsupported metallic samples therefore allows DFT-modeling to be applied to powder catalyst analysis.

Our calculated binding energies for CO adsorption on Pd(111) are similar to previous theoretical work^{31,50} and predict that the energies, corrected for GGA overbinding, for the top, bridge, hollow-fcc, and hollow-hcp sites are 1.23, 1.51, 1.62, and 1.64 eV, respectively. We note that the overbinding correction only reduces the DFT binding energies by ~0.2–0.4 eV but does not affect the prediction of the preferred CO binding site on Pd(111). Thus, the hollow sites are predicted to be the preferred CO binding sites in agreement with experiment^{51,52} and previous theoretical work.^{31,50} The experimental CO binding energies are in the range of 1.47–1.54 eV,^{51,52} whereas previous theoretical work found 1.37³¹ and 1.602 eV.⁵⁰ Differences between computational results are likely due to the use of different exchange correlation functional. In contrast to CO adsorption on Pd(111) we find that the CO binding energies on PdZn(111) are significantly lower.

The computations predict that CO binds most strongly atop Pd sites, the least favorable CO binding site on Pd(111), with a (overbinding corrected) binding energy of only 0.69 eV. The only other energetically favorable binding was found to be the Pd–Pd bridge site, with a (corrected) binding energy of 0.56 eV. Simulations that were initiated with CO atop Zn were found to be unstable. The reduced number of binding sites in PdZn(111) compared to Pd(111) that is due to binding on Pd only and replacement of half the surface with Zn is consistent with previous theoretical work.⁵⁰ We note that our predicted binding energies are systematically lower due to the applied overbinding correction as compared to previous theoretical work.^{50,52}

In summary our calculations corroborate our experimental observations that TPD peak temperatures on PdZn are lower than on metallic Pd. Furthermore, the validity of counting Pd sites using CO chemisorption and CO-oxidation is confirmed since calculations confirm that CO binding on PdZn(111) is similar to CO binding on Pd(111) and occurs only on the Pd sites of PdZn(111). Assuming that a similar relationship holds between other pairs of corresponding surfaces, the DFT calculations predict that the area under the TPD desorption peak and thus adsorbate coverage and reaction site density (for powders and single crystals) decreases with increasing Zn content of PdZn. This prediction corroborates our TPD experiments. Further experimental and theoretical work is needed to better understand the effect of increasing Zn content on the identity and nature of the binding site, site density, binding energies, and reaction pathway energetics for CH₃OH and MSR on PdZn.

Conclusions

An aerosol-derived unsupported model catalyst PdZn was prepared for the study of the specific reactivity of the PdZn phase in MSR. Characterization of the powder model catalyst using XRD, EDS/SEM, EDS/STEM, XRF, and XPS established the powder to be bulk phase pure, with homogeneous composi-

tion throughout the powder and 2–3 monolayers of ZnO on the surface as determined by ambient pressure XPS. The observation of some ZnO on the surface is a consequence of the high reactivity of Zn toward oxygen. However, since reactivity studies used higher hydrogen partial pressures and longer reduction times than those used for the AP-XPS study, it is likely that the 2–3 ML of surface ZnO can be easily reduced as seen from the HRTEM images. The exact nature of the PdZn surface during reaction will be the subject of future investigations. The PdZn powder was tested for methanol steam reforming and CO oxidation reactivity in a flow reactor at atmospheric pressure. The specific reactivity of the PdZn was determined and the observed values for TOF of 0.21 s⁻¹ at 250 °C for MSR and the CO oxidation TOF of 0.06 s⁻¹ at 185 °C are consistent with the literature. Further, the ability to switch from MSR to CO oxidation rapidly without loss of activity demonstrates the inherent stability of the PdZn intermetallic under different chemical environments. These aerosol-derived unsupported intermetallic single phase alloy powders are therefore uniquely useful model catalysts for bridging the gap between well-defined single crystal model catalysts and industrially relevant supported technical catalysts. While thin film alloys have been proposed as suitable analogs for the study of multimetallic catalysts, there are questions about whether their behavior truly mimics supported catalysts. We show here that the catalytic behavior, particularly the product distribution, of the bulk intermetallic powder agrees very well with the supported PdZn catalysts reported in the literature. The ability to explicitly measure the reactivity of an unsupported phase pure metallic powder under flowing gas in atmospheric pressures provides a unique benchmark for future studies of the role of particle size and support on the reactivity of complex multimetallic catalysts.

Acknowledgment. We gratefully acknowledge funding for this work provided by the U.S. Department of Energy Grant No. DE-FG02-05ER15712 and partial funding from Grant DE-FG02-08ER46530 and NSF Grant OISE 0730277. We also gratefully acknowledge computing resources provided by the New Mexico Computing Applications Center (NMCAC) on Encanto. Ambient pressure XPS experiments were carried out at BESSY II, Helmholtz-Zentrum Berlin. A portion of the research was performed using EMSL, a national scientific user facility sponsored by the Department of Energy's Office of Biological and Environmental Research and located at Pacific Northwest National Laboratory. Lastly, we thank Ron Goeke at Sandia National Laboratories, Albuquerque for helpful discussions and analysis. The work was inspired by the work of Professor D. Wayne Goodman on the development of model catalysts.

Note Added after ASAP Publication. This paper was published on the Web on September 3, 2010, with an error to Figure 6. The corrected version was reposted on September 9, 2010.

References and Notes

- (1) Alexeev, O. S.; Gates, B. C. Supported Bimetallic Cluster Catalysts. *Ind. Eng. Chem. Res.* **2002**, 42 (8), 1571–1587.
- (2) Sinfelt, J. H. *Bimetallic Catalysts: Discoveries, Concepts, and Applications*; Wiley: New York, 1983.
- (3) Rodriguez, J. A.; Goodman, D. W. The Nature of the Metal Metal Bond in Bimetallic Surfaces. *Science* **1992**, 257 (5072), 897–903.
- (4) Rodriguez, J. A.; Goodman, D. W. High-Pressure Catalytic Reactions over Single-Crystal Metal-Surfaces. *Surf. Sci. Rep.* **1991**, 14 (1–2), 1–107.

- (5) Rodriguez, J. A.; Goodman, D. W. Surface Science Studies of the Electronic and Chemical-Properties of Bimetallic Systems. *J. Phys. Chem.* **1991**, *95* (11), 4196–4206.
- (6) Sinfelt, J. H. Role of surface science in catalysis. *Surf. Sci.* **2002**, *500* (1–3), 923–946.
- (7) Gao, F.; et al. CO Oxidation on Pt-Group Metals from Ultrahigh Vacuum to Near Atmospheric Pressures. 2. Palladium and Platinum. *J. Phys. Chem. C* **2009**, *113* (1), 174–181.
- (8) Valden, M.; Lai, X.; Goodman, D. W. Onset of catalytic activity of gold clusters on titania with the appearance of nonmetallic properties. *Science* **1998**, *281* (5383), 1647–1650.
- (9) Rameshan, C.; et al. Subsurface-Controlled CO₂ Selectivity of PdZn Near-Surface Alloys in H₂ Generation by Methanol Steam Reforming. *Angew. Chem., Int. Ed.* **2010**, *49* (18), 3224–3227.
- (10) Stadlmayr, W.; et al. Temperature-Induced Modifications of PdZn Layers on Pd(111). *J. Phys. Chem. C* **2010**, *114* (24), 10850–10856.
- (11) Iwasa, N.; et al. Steam Reforming of Methanol over Pd/ZnO - Effect of the Formation of PdZn Alloys Upon the Reaction. *Appl. Catal., A* **1995**, *125* (1), 145–157.
- (12) Iwasa, N.; Masuda, S.; Takezawa, N. Steam Reforming Of Methanol Over Ni, Co, Pd And Pt Supported On ZnO. *React. Kinet. Catal. Lett.* **1995**, *55* (2), 349–353.
- (13) Iwasa, N.; et al. Highly Selective Supported Pd Catalysts For Steam Reforming Of Methanol. *Catal. Lett.* **1993**, *19* (2–3), 211–216.
- (14) Iwasa, N.; et al. Selective PdZn alloy formation in the reduction of Pd/ZnO catalysts. *Bull. Chem. Soc. Jpn.* **1998**, *71* (6), 1451–1455.
- (15) Karim, A.; Conant, T.; Datye, A. The role of PdZn alloy formation and particle size on the selectivity for steam reforming of methanol. *J. Catal.* **2006**, *243* (2), 420–427.
- (16) Karim, A. M.; Conant, T.; Datye, A. K. Controlling ZnO morphology for improved methanol steam reforming reactivity. *Phys. Chem. Chem. Phys.* **2008**, *10* (36), 5584–5590.
- (17) Lebarbier, V.; et al. The effect of PdZn particle size on reverse-water-gas-shift reaction. *Appl. Catal., A* **2010**, *379* (1–2), 3–6.
- (18) Conant, T.; et al. Stability of bimetallic Pd-Zn catalysts for the steam reforming of methanol. *J. Catal.* **2008**, *257* (1), 64–70.
- (19) Peterson, E. J.; et al. Aerosol synthesis and Rietveld analysis of tetragonal (b1) PdZn. *J. Alloys Compd.* **2010**.
- (20) Hohenberg, P.; Kohn, W. Inhomogeneous Electron Gas. *Phys. Rev. B* **1964**, *136* (3B), B864.
- (21) Kresse, G.; Furthmuller, J. Efficiency of ab-initio total energy calculations for metals and semiconductors using a plane-wave basis set. *Comput. Mater. Sci.* **1996**, *6* (1), 15–50.
- (22) Kresse, G.; Hafner, J. Ab-Initio Molecular-Dynamics for Open-Shell Transition-Metals. *Phys. Rev. B* **1993**, *48* (17), 13115–13118.
- (23) Kresse, G.; Hafner, J. Norm-Conserving and Ultrasoft Pseudopotentials for First-Row and Transition-Elements. *J. Phys.: Condens. Matter* **1994**, *6* (40), 8245–8257.
- (24) Kresse, G.; Furthmuller, J. Efficient iterative schemes for ab initio total-energy calculations using a plane-wave basis set. *Phys. Rev. B* **1996**, *54* (16), 11169–11186.
- (25) Perdew, J. P.; Burke, K.; Ernzerhof, M. Generalized gradient approximation made simple. *Phys. Rev. Lett.* **1996**, *77* (18), 3865–3868.
- (26) Blochl, P. E. Projector Augmented-Wave Method. *Phys. Rev. B* **1994**, *50* (24), 17953–17979.
- (27) Kresse, G.; Joubert, D. From ultrasoft pseudopotentials to the projector augmented-wave method. *Phys. Rev. B* **1999**, *59* (3), 1758–1775.
- (28) Nowotny, H.; Bittner, H. *Die Kristallstruktur Von Pdzn. *Monahts. Chem.* **1950**, *81* (5), 679–680.
- (29) Chen, Z. X.; et al. Surface structure and stability of PdZn and PtZn alloys: Density-functional slab model studies. *Phys. Rev. B* **2003**, *68* (7), 8.
- (30) Bredig, G.; Allolio, R. Radiation investigations in catalytic effecting metals. *Z. Phys. Chem.* **1927**, *126* (1/2), 41–71.
- (31) Abild-Pedersen, F.; Andersson, M. P. CO adsorption energies on metals with correction for high coordination adsorption sites - A density functional study. *Surf. Sci.* **2007**, *601* (7), 1747–1753.
- (32) Makov, G.; Payne, M. C. Periodic Boundary-Conditions in Ab-Initio Calculations. *Phys. Rev. B* **1995**, *51* (7), 4014–4022.
- (33) Neugebauer, J.; Scheffler, M. Adsorbate-Substrate and Adsorbate-Adsorbate Interactions of Na and K Adlayers on Al(111). *Phys. Rev. B* **1992**, *46* (24), 16067–16080.
- (34) Methfessel, M.; Paxton, A. T. High-Precision Sampling for Brillouin-Zone Integration in Metals. *Phys. Rev. B* **1989**, *40* (6), 3616–3621.
- (35) Blyholder, G. Molecular Orbital View of Chemisorbed Carbon Monoxide. *J. Phys. Chem.* **1964**, *68* (10), 2772–2777.
- (36) Ertl, G. *Handbook Of Heterogeneous Catalysis*, 2nd ed.; Wiley-VCH Verlag GmbH & Co.: Weinheim, Germany, 2008; Vol. 3.
- (37) Ketteler, G.; et al. In Situ Spectroscopic Study of the Oxidation and Reduction of Pd(111). *J. Am. Chem. Soc.* **2005**, *127* (51), 18269–18273.
- (38) Salmeron, M.; Schlogl, R. Ambient pressure photoelectron spectroscopy: A new tool for surface science and nanotechnology. *Surf. Sci. Rep.* **2008**, *63* (4), 169–199.
- (39) Stadlmayr, W.; et al. Temperature-Induced Modifications of PdZn Layers on Pd(111). *J. Phys. Chem. C* **2010**, *114* (24), 10850–10856.
- (40) Moulder, J. F. *Handbook of X-Ray Photoelectron Spectroscopy*; Physical Electronics Inc.: Eden Prairie, MN, 1995.
- (41) Bayer, A.; et al. Electronic properties of thin Zn layers on Pd(111) during growth and alloying. *Surf. Sci.* **2006**, *600* (1), 78–94.
- (42) Penn, D. R. Quantitative Chemical-Analysis By Esca. *J. Electron Spectrosc. Relat. Phenom.* **1976**, *9* (1), 29–40.
- (43) Jeroro, E.; et al. Interaction of CO with surface PdZn alloys. *Surf. Sci.* **2007**, *601* (23), 5546–5554.
- (44) Jeroro, E.; Vohs, J. M. Zn modification of the reactivity of Pd(111) toward methanol and formaldehyde. *J. Am. Chem. Soc.* **2008**, *130* (31), 10199–10207.
- (45) Ranganathan, E. S.; Bej, S. K.; Thompson, L. T. Methanol steam reforming over Pd/ZnO and Pd/CeO₂ catalysts. *Appl. Catal., A* **2005**, *289* (2), 153–162.
- (46) Amphlett, J. C.; et al. Hydrogen-Production By The Catalytic Steam Reforming Of Methanol 0.2. Kinetics Of Methanol Decomposition Using Girdler G66b Catalyst. *Can. J. Chem. Eng.* **1985**, *63* (4), 605–611.
- (47) Jiang, C. J.; et al. Kinetic Mechanism For The Reaction Between Methanol And Water Over A Cu-ZnO-Al₂O₃ Catalyst. *Appl. Catal., A* **1993**, *97* (2), 145–158.
- (48) Jiang, C. J.; et al. Kinetic-Study Of Steam Reforming Of Methanol Over Copper-Based Catalysts. *Appl. Catal., A* **1993**, *93* (2), 245–255.
- (49) Cant, N. W.; Hicks, P. C.; Lennon, B. S. Steady-state oxidation of carbon monoxide over supported noble metals with particular reference to platinum. *J. Catal.* **1978**, *54* (3), 372–383.
- (50) Mason, S. E.; Grinberg, I.; Rappe, A. M. First-principles extrapolation method for accurate CO adsorption energies on metal surfaces. *Phys. Rev. B* **2004**, *69* (16), 161401.
- (51) Guo, X. C.; Yates, J. T. Dependence of Effective Desorption Kinetic-Parameters on Surface Coverage and Adsorption Temperature - Co on Pd(111). *J. Chem. Phys.* **1989**, *90* (11), 6761–6766.
- (52) Conrad, H.; et al. Adsorption of Co on Pd Single-Crystal Surfaces. *Surf. Sci.* **1974**, *43* (2), 462–480.

JP103967X